Acceleration statistics of solid particles in turbulent channel flow

Rémi Zamansky, Ivana Vinkovic, Mikhael Gorokhovski

AIP | Physics of Fluids

Acceleration statistics of solid particles in turbulent channel flow

R. Zamansky, I. Vinkovic, and M. Gorokhovski

Citation: Phys. Fluids **23**, 113304 (2011); doi: 10.1063/1.3662006
View online: http://dx.doi.org/10.1063/1.3662006
View Table of Contents: http://pof.aip.org/resource/1/PHFLE6/v23/i11
Published by the American Institute of Physics.

Acceleration statistics of solid particles in turbulent channel flow

R. Zamansky, I. Vinkovic,[a] and M. Gorokhovski
Laboratoire de Mécanique des Fluides et d'Acoustique, Université de Lyon, Université Claude Bernard Lyon 1, Ecole Centrale de Lyon, INSA de Lyon, CNRS UMR 5509, 36 Avenue Guy de Collongue, F-69134 Ecully, France

(Received 24 February 2011; accepted 12 October 2011; published online 28 November 2011)

Direct numerical simulations (DNS) are used here to study inertial particle acceleration statistics in the near-wall region of a turbulent channel flow. The study is motivated by observations in homogeneous isotropic turbulence (HIT) suggesting that when particle inertia increases, particle acceleration variance decreases due to both particle preferential accumulation and the filtering effect of inertia. In accordance with these studies, the present DNS shows that for increasing inertia, solid particle acceleration probability density functions (PDFs), scaled by the acceleration root-mean-square (RMS), depart from that of the fluid. The tails of these PDFs become narrower. However, in turbulent channel flow, as the Stokes number increases up to 5, the streamwise acceleration RMS in the near-wall region increases, while further increase of the Stokes number is characterized by the streamwise acceleration RMS decrease. In parallel, contrary to calculations in homogeneous isotropic turbulence, the conditional acceleration statistics of the fluid seen by the solid particle show that while the vertical and transverse acceleration RMS components remain close to the unconditional fluid acceleration, the longitudinal RMS component is remarkably higher in the near wall region. This feature is more pronounced as the Stokes number is increased. Additionally, the conditional acceleration PDFs overlap almost perfectly with the unconditional fluid PDFs, normalized by the acceleration RMS. The enhanced longitudinal acceleration variance of the fluid seen by the particles may be due to the spanwise alternation of high-and-low speed streaks. Depending on inertia, particles may respond to those fluid solicitations (experiencing an increase of the longitudinal acceleration RMS) or ignore the wall turbulent structures (presenting in that case a more homogeneous concentration). © *2011 American Institute of Physics*. [doi:10.1063/1.3662006]

I. INTRODUCTION

Understanding the Lagrangian behavior of inertial particles in turbulent channel flows has important implications for many environmental systems, from sediment transport to atmospheric dispersion of pollutants or solid deposition in marine flows. Previous experimental[1–4] and numerical[5,6] studies on particle-laden channel flows have examined particle deposition, trapping, segregation, and the modification of particle velocity statistics due to the presence of coherent structures. It is recognized that inertial effects cause particle segregation and clustering.[2,7] In Refs. 8–10 these phenomena are linked to the particle acceleration. An adequate description of acceleration statistics is essential for the modelling of solid particle dispersion[11] and droplet breakup.[12] Acceleration statistics of the fluid along the particle path are also of crucial significance in turbulent spray vaporization and combustion.[13]

Recently, significant advances have been made in the measurement of particle trajectories in turbulence. These have been due to experimental developments in high-speed tracking devices,[14–16] and in generating devices for high Reynolds number turbulent flows. At the same time, increasing computational resources enabled moderate Reynolds number direct numerical simulations (DNS) of dispersed flows in homogeneous isotropic cases[9] as well as in wall-bounded configurations.[5,17] Lagrangian measurements or computations provided insight into inertial particle accelerations and their statistics, including the acceleration probability density functions (PDF), in both homogeneous and inhomogeneous flows. In computations of turbulent dispersed flows, it is usually assumed that the flow is uniform on the particle length scale. In that case, the acceleration of a spherical non-rotating heavy particle $\vec{a}_p$, with diameter d_p, is governed by the Stokes law: $\vec{a}_p = \vec{u}_{\rm rel}/\tau_p + \vec{g}$, where $\vec{u}_{\rm rel}$ is the relative fluid-to-particle velocity, τ_p is the particle velocity response time, and $\vec{g}$ is the acceleration due to gravity (here, the buoyancy force is not included and the drag coefficient is taken as unity). In homogeneous isotropic turbulence (HIT), the statistically stationary estimate of $\overline{u_{\rm rel}^2}$ along the path of inertial particles[18] shows that when τ_p belongs to the inertial subrange of timescales, one has $\sqrt{\overline{u_{\rm rel}^2}} \sim \sqrt{\bar{\varepsilon}\tau_p}$, where $\bar{\varepsilon}$ is the mean dissipation rate. The acceleration variance is then scaled as $\sqrt{\overline{a_p^2}} \sim \sqrt{\bar{\varepsilon}/\tau_p}$. Its decrease with increasing response time is often referred to as the "filtering" effect of particle inertia. When τ_p is less than the Kolmogorov's timescale, $\tau_\eta \sim \sqrt{\nu/\bar{\varepsilon}}$, the estimate of $\overline{u_{\rm rel}^2}$ shows that $u_{\rm rel}/u' \ll 1$, i.e., along the particle's trajectory, the acceleration statistics of the particle coincide with the acceleration statistics of the fluid particle. If the Reynolds number is high, the latter can be

[a]Electronic mail: ivana.vinkovic@univ-lyon1.fr.

strongly intermittent, with stretched tails in the acceleration PDF.[15,16] However, with increasing inertia, particles that are denser than the surrounding fluid are likely to be centrifuged out of intense vortices. Additionally to the filtering effect, this leads to another effect of particle inertia: the particle's acceleration variance may be reduced due to longer residence time in the low-vorticity (high-strain) regions. This effect is referred to as the preferential accumulation of particles.[19]

The acceleration dynamics of heavy particles in HIT were recently explored by Bec *et al.*[9] by means of direct numerical simulations (DNS) with Lagrangian tracking of inertial particles. Bec *et al.*[9] observed that solid particles with low inertia exhibit highly non-Gaussian acceleration PDFs with a high probability of intense acceleration events. The tails of these acceleration PDFs narrow and the PDFs tend towards Gaussianity as particle inertia increases.[9] Bec *et al.*[9] showed that the trend of acceleration PDFs towards Gaussianity, as well as a monotonic decrease of acceleration variance, are both a consequence of the preferential accumulation (dominant at small Stokes numbers) and filtering due to particle inertia (for particles with larger Stokes numbers).

Ayyalasomayajula *et al.*[10] measured inertial particle (water droplets) accelerations in a grid generated wind tunnel turbulence. They found that the normalized droplet acceleration PDFs have heavy tails. These tails are less extended than those of a fluid particle. The authors also observed that there is a decrease in inertial particle acceleration variance with increasing the Stokes number. Through a simple vortex model for isotropic turbulence, Ayyalasomayajula *et al.*[10] illustrated that inertial particles preferentially accumulate in regions of the fluid undergoing low accelerations. They stated that, at low Stokes numbers, the preferential accumulation of particles is responsible for the reduction in the acceleration variance and partially explains the attenuation of the tails of the acceleration PDF.

One could expect similar tendencies in the presence of the wall: the preferential accumulation and the filtering effect due to particle inertia may decrease the variance of particle acceleration. Gerashchenko *et al.*[20] were amongst the first to measure inertial particle acceleration using high-speed Lagrangian tracking techniques in a boundary layer flow forced by free-stream turbulence. Contrary to the trend found in HIT, Gerashchenko *et al.*[20] showed that the variance of inertial particle accelerations in the near-wall region increases with inertia. Gerashchenko *et al.*[20] put emphasis on the shear effect in the wall-region: more inertial particles settled towards the wall are subjected to stronger deceleration due to the mean shear. This issue was further investigated by Lavezzo *et al.*,[17] who performed DNS of channel flow with dispersed particles tracked in the Lagrangian frame of reference. By comparing the simulations with and without gravity, Lavezzo *et al.*[17] confirmed the experimental observations of Gerashchenko *et al.*,[20] pointing out the dominant contribution of gravitational settling in the coupling between mean shear and particle inertia.

The emphasis in our study is placed on the role of the wall boundary layer structures in particle acceleration statistics. We draw the following picture. Near the wall region there are high-and-low speed streaks, aligned with the wall and alternating in the spanwise direction in the wall plane. In the near-wall region, particles are submitted to this spanwise alternation. Low-inertia particles do not sample the alternation of regions; they tend to travel along with the surrounding fluid. Highly inertial particles neither respond to this intermittency, due to the filtering effect. Only particles with intermediate inertia are subjected to longitudinal accelerations and decelerations. This picture motivated our research in lines of the DNS of Lavezzo *et al.*,[17] but without gravity, with a twice higher Reynolds number and another range of Stokes numbers. Additionally, fluid acceleration statistics conditioned on the inertial particle position are analyzed here. For a chosen range of the Stokes numbers from 1 to 25, we observe that close to the wall, particles with increasing inertia are surrounded by fluid with an increasing acceleration variance. Within this range of Stokes numbers, there is a given subrange, in which particles along their paths respond to the intermittency of high-and-low speed streaks, resulting in an increased particle acceleration variance. In this paper, the PDF of the fluid acceleration seen by inertial particles exhibits a universal shape for the chosen range of Stokes numbers, with acceleration variance as the scaling parameter.

This paper is organized as follows. The governing equations and parameters are presented in Sec. II. Some aspects of the numerical simulations are described in Sec. III. Comparisons with other studies, results on the acceleration statistics and the discussion are given in Sec. IV. Finally, the conclusions are presented in Sec. V.

II. GOVERNING EQUATIONS

A. Flow

The flow considered is an incompressible turbulent channel flow. The governing equations for the fluid in dimensionless form are given by the Navier-Stokes equations

$$\vec{\nabla}\cdot\vec{u}=\vec{0}, \tag{1}$$

$$\frac{\partial\vec{u}}{\partial t}+\left(\vec{\nabla}\times\vec{u}\right)\times\vec{u}+\vec{\nabla}\left(\frac{p}{\rho}+\frac{u^2}{2}\right)-\frac{1}{Re}\Delta\vec{u}=-\frac{1}{\rho}\vec{\nabla}p_0, \tag{2}$$

where $\vec{u}$ is the velocity vector, p is the fluctuating pressure, ρ is the fluid density, and $-\vec{\nabla}p_0$ is the prescribed constant pressure drop. In the following, the velocity components along the x (streamwise), y (vertical), and z (transverse) directions will be denoted by u, v, and w, respectively. Re is the Reynolds number based on the mean velocity U at the center of the channel, the channel half height h and the kinematic viscosity ν.

The computational domain consisting of two infinite parallel walls is illustrated in Figure 1. Periodic boundary conditions are imposed on the fluid velocity field in x and z directions and no-slip boundary conditions are imposed at the walls.

B. Particles

Particles are injected into the flow at low volume fractions ($\Phi_v<10^{-6}$). Particle-particle interactions and the influence of particles on the carrier fluid are neglected given

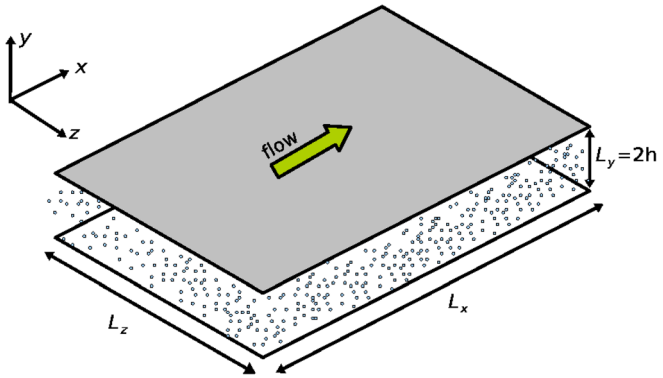

FIG. 1. (Color online) Channel flow. x, y, z represent the streamwise, the vertical and the transverse directions, respectively.

these low volume fractions. Gravity is also not accounted for. Each particle that impacts the wall (considered as perfectly smooth) rebounds elastically. Particles are considered to be pointwise, spherical, rigid, and to obey the following Lagrangian dimensionless equation of motion

$$St\frac{d\vec{v}_p}{dt} = (\vec{u} - \vec{v}_p)f(Re_p), \tag{3}$$

$$\frac{d\vec{x}_p}{dt} = \vec{v}_p. \tag{4}$$

Here, $\vec{v}_p$ and $\vec{x}_p$ are the dimensionless particle velocity and position. The solid-particle fluid interaction is modelled by a drag force with the correction term $f(Re_p) = 1 + 0.15Re_p^{0.687}$ proposed by Clift *et al.*[21] There, Re_p is the local and instantaneous particle Reynolds number based on the local relative velocity, the particle diameter d_p and the fluid viscosity. St is the Stokes number given by

$$St = \frac{\tau_p}{\tau_f}, \tag{5}$$

with $\tau_p = \frac{\rho_p d_p^2}{18\rho\nu}$ and $\tau_f = \frac{\nu}{u_*^2}$, ρ_p being the particle density. The Stokes number characterizes the response time of a particle to fluid solicitation.

Four sets of particles are considered. The characteristics of the particles are given in Table I, where $d_p^+ = d_p u_*/\nu$ is the particle diameter normalized by the friction velocity u_* and the viscosity ν. It should be noted that since the particles are treated as points, their diameter and the volume fraction do not enter into the calculation.

III. NUMERICAL SIMULATION

The incompressible Navier-Stokes equations in a turbulent channel flow are solved using a Galerkin spectral approximation (Fourier Chebyshev) and a variational projection method in a divergence free space as described by Pascal[22] and Buffat *et al.*[23] This DNS code has been successfully applied previously by Laadhari.[24,25] Steady state fluid statistics have been compared with the results of Moser *et al.*[26] and Hoyas and Jiménez.[27] Details on this comparison may be found in Zamansky *et al.*[28]

TABLE I. Characteristics of particles.

St	d_p^+	ρ_p/ρ	Φ_v
1	0.15	770	7×10^{-8}
5	0.34	770	8×10^{-7}
15	0.59	770	4×10^{-7}
25	0.76	770	9×10^{-7}

The calculations are performed for $Re \sim 12\,500$. Details of the simulation characteristics are given in Table II, where N_i and L_i are the number of grid points and the domain length in direction i. Typical space and time step values are also given. $Re_\tau = u_* h/\nu$ is the Reynolds number based on the friction velocity u_*. The superscript "+" denotes quantities expressed in wall units, normalized by the friction velocity u_*, and the viscosity ν.

Once the steady state for statistics of the fluid is obtained, particles are released at uniformly random locations within the channel, and then tracked at each time step. The initial velocities of the particles are set equal to the interpolated fluid velocities at each particle location. A high-order three-dimensional Hermite interpolation is used for computing the fluid velocity $\vec{u}(\vec{x}_p, t)$ at the particle position. The time-integration of the particle motion Eq. (3) is performed using a second-order Adams-Bashforth method with the same time step as the DNS. Once the particles released, the simulations are run over several particle timescales τ_p. Particle statistics are sampled starting from $t^+ \sim 1000$, counted from particle release. For all simulations, velocity statistics for the solid phase are at the stationary state.

In this study, the acceleration is evaluated using the velocity time derivative along particle trajectories. Even though we use a three-dimensional Hermite interpolation for computing the fluid velocity at particle position, as suggested by Choi *et al.*,[29] numerical errors are generated when a particle crosses a grid point. Using different sets of data to obtain the fluid velocity before and after the particle crosses a grid point causes discontinuous time-derivative. This gives rise to undesirable errors in Lagrangian statistics for the acceleration. Therefore, as suggested by Mordant *et al.*,[30] the acceleration is estimated by a convolution of the Lagrangian velocity with the derivative of a Gaussian kernel. The filter width, of the order of τ_f, is such that there is agreement between fluid Lagrangian and Eulerian acceleration statistics.

IV. RESULTS AND DISCUSSION

A. Solid particle acceleration statistics

1. Comparison with other studies

Hereafter, we discuss the comparison with the DNS of Yeo *et al.*,[31] the experiments of Gerashchenko *et al.*,[20] and the DNS of Lavezzo *et al.*[17] Yeo *et al.*[31] studied fluid acceleration statistics, whereas Gerashchenko *et al.*[20] and Lavezzo *et al.*[17] analyzed the acceleration statistics of inertial particles. For a lower Reynolds number, particle velocity statistics have been compared with the benchmark test proposed by Marchioli *et al.*[32] For higher Reynolds numbers, velocity statistics have also been compared to experiments.[4] Details

TABLE II. Characteristics of the numerical simulations.

	Re_τ	Re	$N_x \times N_y \times N_z$	$L_x \times L_y \times L_z$	$\Delta x^+ \times \Delta y^+ \times \Delta z^+$	dt^+
DNS	587	12 490	$384 \times 257 \times 384$	$\frac{3}{2}\pi h \times 2h \times \frac{3}{4}\pi h$	$7.2 \times (0.04 \sim 7.2) \times 3.6$	0.033

about these comparisons and other results based on particle velocity statistics may be found in Vinkovic *et al.*[6]

The mean profiles of the x and y acceleration of solid particles are shown in Figure 2. For comparison, the corresponding acceleration profiles of the fluid obtained by the DNS of Yeo *et al.*[31] and by our DNS are presented. Yeo *et al.*[31] studied the behavior of fluid acceleration near the wall in a turbulent channel flow at $Re_\tau = 180 \sim 600$ without gravity. We use their results obtained at $Re_\tau = 600$, which corresponds to the Re_τ of our DNS. It is seen that our DNS is

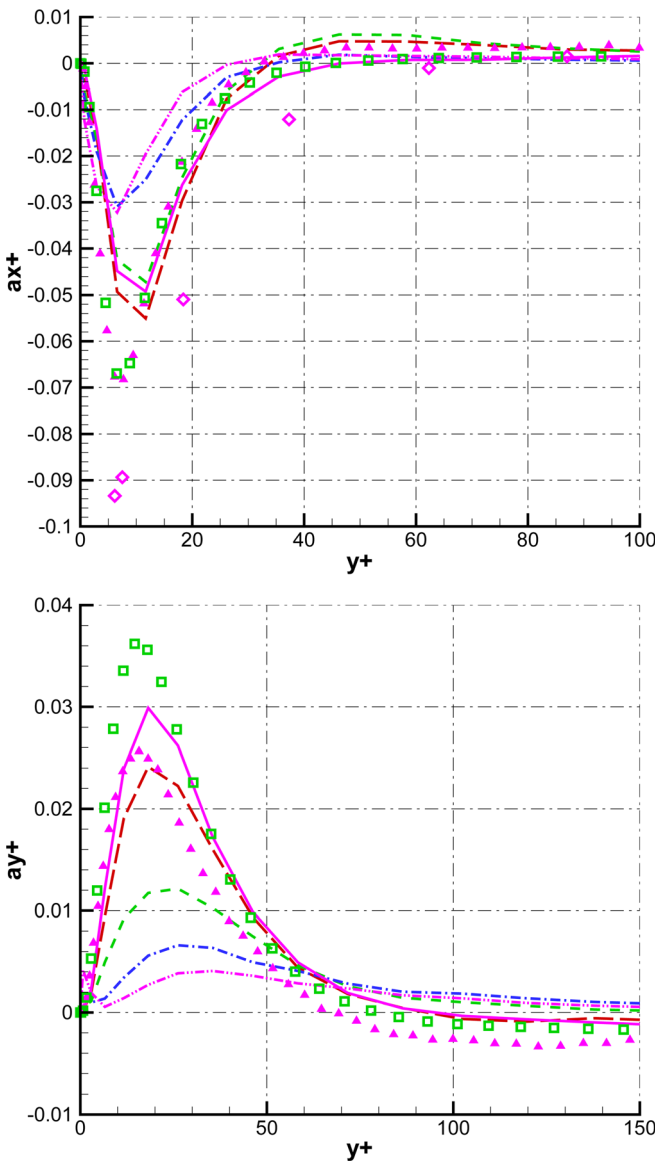

FIG. 2. (Color online) Mean acceleration profile of the x (up) and the y (bottom) components: $St = 1$ (long dashed), $St = 5$ (dashed), $St = 15$ (dashed and dotted), $St = 25$ (dashed and dotted-dotted), fluid (line), Gerashchenko *et al.* (Ref. 20) for $St \sim 0.7$ and $Re_\tau \sim 470$ (diamonds), Lavezzo *et al.* (Ref. 17) for $St = 0.87$ and $Re_\tau = 300$ (full triangles), Yeo *et al.* (Ref. 31) for fluid particles at $Re_\tau = 600$ (squares).

in agreement with the DNS of Yeo *et al.*[31] for both acceleration components, except a slight difference in the peak prediction of the average acceleration profile.

The measurements reported by Gerashchenko *et al.*[20] for inertial particles in the turbulent boundary layer are also presented in Figure 2. The case of $Re_{\lambda 0} = 100$ and $St_0 = 0.035$ is plotted; where $Re_{\lambda 0}$ is the Reynolds number based on the Taylor-scale and the streamwise velocity root-mean-square (RMS), and where the subscript zero refers to the free-stream conditions. This corresponds to $Re_\tau \sim 470$ and $St \sim 0.7$ and is closest to our $St = 1$ and $Re_\tau \sim 600$ simulation. For the x component of the mean acceleration, it is seen that our numerical data are in agreement with the experimental profile except in the near-wall region. Here, our simulations underpredict the negative peak in the mean longitudinal acceleration. For the y component of the mean acceleration, Gerashchenko *et al.*[20] measured negative values in the near-wall region. Our simulations predict a positive acceleration. The reason for this is that in the experiments,[20] gravity was conjectured as a significant factor in the mean particle acceleration, whereas in our simulations, gravity is neglected. Addressing the DNS results of Lavezzo *et al.*,[17] also shown in Figure 2 for the case without gravity, $St = 0.87$ and $Re_\tau = 300$, it can be seen that the particle mean acceleration components in the present DNS are close to those of Lavezzo *et al.*[17]

The RMS longitudinal and vertical acceleration of solid particles as a function of y^+ are presented in Figure 3. Once again for comparison, the fluid RMS acceleration obtained by our DNS and by the DNS of Yeo *et al.*,[31] the experimental results of Gerashchenko *et al.*[20] and the DNS results of Lavezzo *et al.*[17] are also illustrated. For the fluid, the peak of acceleration RMS obtained in our DNS is lower than the one computed by Yeo *et al.*[31] as is also seen in Figure 2 for the mean acceleration. For both components of the particle acceleration RMS, the DNS results are close to the measurements of Gerashchenko *et al.*[20] although gravity was not taken into account here. Close to the wall, the DNS of Lavezzo *et al.*[17] slightly overestimate the peak of inertial particle acceleration RMS compared to the present DNS.

2. Stokes number influence

It is seen in Figure 2 that as the wall is approached, the mean solid particle accelerations in the streamwise direction become negative, while in the vertical direction, accelerations become positive, as in the DNS of Lavezzo *et al.*[17] The effect is most pronounced in the low-Stokes number case. As the Stokes number increases the solid particle acceleration profiles depart from that of the fluid. Clearly, inertial effects play a significant role. Average solid particle accelerations decrease in absolute value and are more uniformly distributed along the channel.

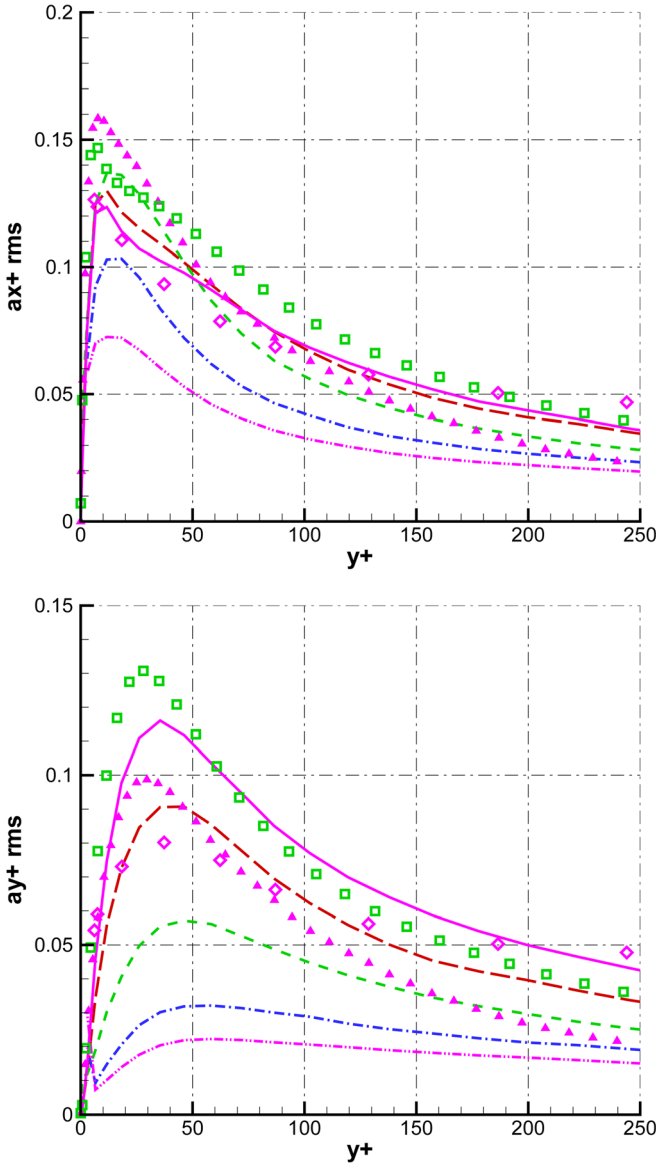

FIG. 3. (Color online) Acceleration RMS profile of the x (up) and the y (bottom) components: $St=1$ (long dashed), $St=5$ (dashed), $St=15$ (dashed and dotted), $St=25$ (dashed and dotted-dotted), fluid (line), Gerashchenko *et al.* (Ref. 20) for $St\sim0.7$ and $Re_\tau\sim470$ (diamonds), Lavezzo *et al.* (Ref. 17) for $St=0.87$ and $Re_\tau=300$ (full triangles), Yeo *et al.* (Ref. 31) for fluid particles at $Re_\tau=600$ (squares).

As already observed by Gerashchenko *et al.*,[20] the y component of the RMS acceleration peaks close to the wall (Figure 3). The position of the peak moves away from the wall as the Stokes number is increased. This is also seen from our DNS in Figure 3. Moreover, whatever the Stokes number, the vertical acceleration RMS is lower in magnitude than the longitudinal one. This is also consistent with Gerashchenko *et al.*[20] Very near the wall ($y^+<10$), for $St=15$ and 25, one can observe a slight peak in vertical acceleration RMS (Figure 3 bottom). This is due to the vertical particle velocity condition on the wall: a particle that strikes the wall rebounds elastically.

Inspection of the solid particle acceleration RMS (Figure 3) shows that far from the wall ($y^+>50$), both vertical and streamwise acceleration RMS monotonically decrease with the Stokes number. This is in accordance with previous DNS in HIT (Refs. 9 and 33) and results from the increase in particle response time with increasing Stokes number. However close to the wall, when the Stokes number is increased from $St=1$ to 5, the peak of the streamwise acceleration RMS increases as well. The further increase of the Stokes number leads to a decrease of the particle acceleration RMS. The peak of the longitudinal acceleration RMS for $St=1$ and 5 is even higher than the local longitudinal acceleration RMS of the fluid. To gain insight in this behavior, the acceleration statistics of the fluid seen by the solid particles will be addressed in Sec. IV B.

3. Particle acceleration PDF

The PDFs of the longitudinal solid particle acceleration are shown in Figure 4 for three different Stokes number values ($St=1$, 5, and 15). The PDFs are obtained from the longitudinal acceleration fluctuation (without the mean value). For each case, four wall distances are presented ($y^+=548$, 244, 72, and 12). At the channel center line ($y^+=548$), the fluid longitudinal acceleration is also shown. For $St=1$, the PDF obtained here at $y^+=244$ is compared to PDF measured in the free-stream by Gerashchenko *et al.*[20] A relatively good qualitative agreement with this experiment is seen. Figure 4 shows that with decreasing y^+, the tail of the x component acceleration PDF becomes narrower. In accordance with Gerashchenko *et al.*,[20] this trend is more pronounced as the Stokes number is increased. The tails of the acceleration PDF of the other two components (not presented here) also narrow as y^+ decreases. At the center of the channel, as expected, when inertia increases the solid particle PDFs depart from the fluid. The tails of these PDFs become narrower. A similar trend has been observed in previous studies in HIT.[9,10,15]

B. Acceleration statistics of the fluid seen by solid particles

Inspection of the solid particle longitudinal acceleration RMS (Figure 3 bottom), shows that for $St=5$, the longitudinal acceleration RMS presents the highest peak close to the wall. This peak is even higher than the fluid longitudinal acceleration RMS. To gain insight in this behavior, we analyze the acceleration statistics of the fluid seen by the solid particles.

1. Acceleration RMS

Figure 5 shows the RMS of the solid particle acceleration, the fluid acceleration sampled by the solid particles and the unconditional fluid acceleration for the longitudinal and vertical components. If we compare the acceleration RMS of the fluid seen by solid particles and of the unconditional fluid, the streamwise and vertical components exhibit different behaviors. For the longitudinal component, the RMS acceleration of the fluid, seen by the solid particles, is higher than the RMS of the unconditional fluid. This is specially pronounced in the near wall region. For the vertical component, the RMS acceleration of the fluid seen by the particles

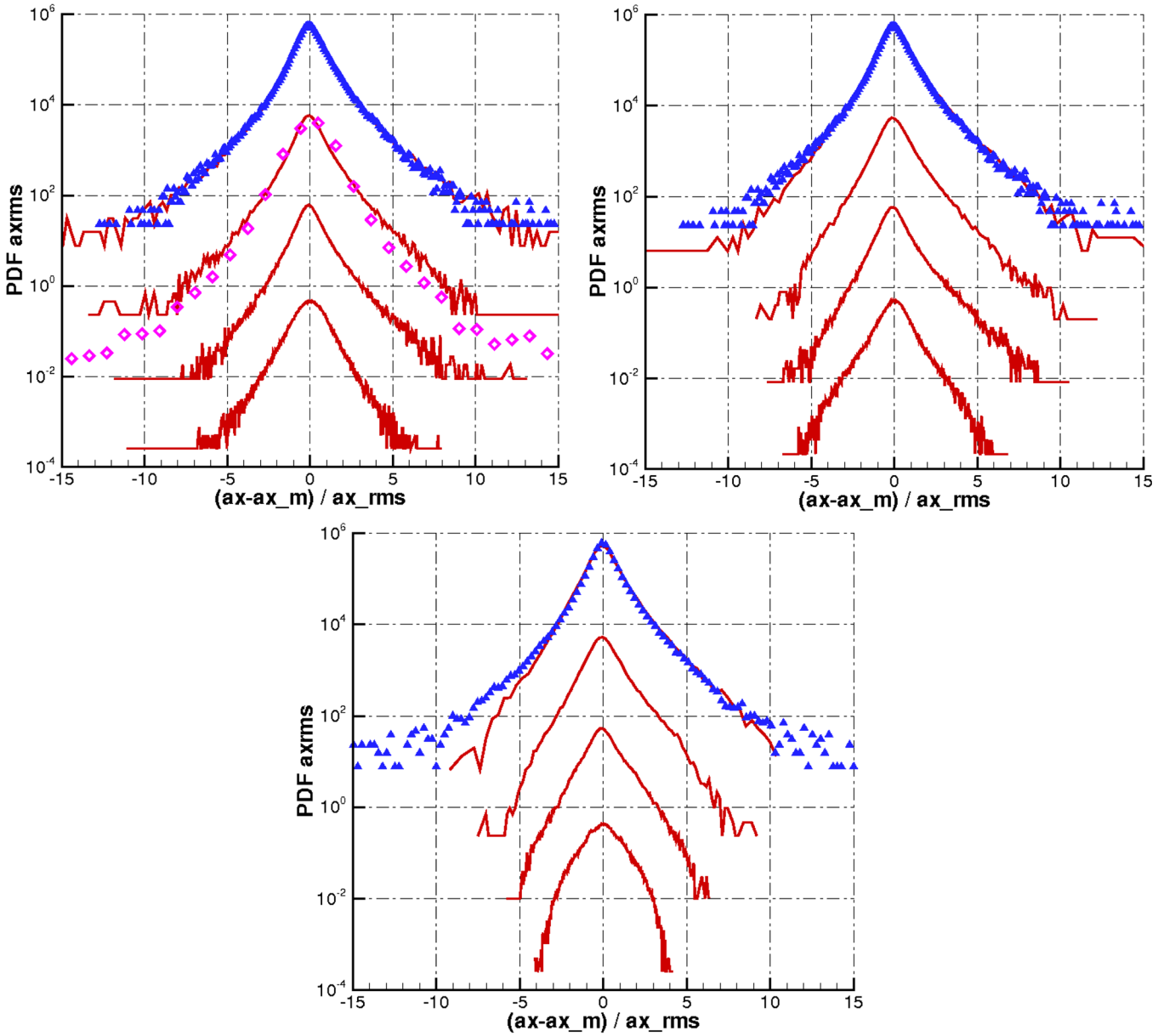

FIG. 4. (Color online) Normalized PDFs of longitudinal acceleration for $St = 1$ (up left), $St = 5$ (up right), and $St = 15$ (bottom). For each plot from top to bottom: $y^+ = 548$, 244, 72, and 12. All plots are shifted up by 100 units. Solid particles (line), fluid (triangles), Gerashchenko *et al*. (Ref. 20) (diamonds).

is close to the value of the unconditional fluid. The transverse component of the RMS presents the same behavior as the vertical one. For clarity of presentation, this component is not shown in the paper. It is seen that the peak value of fluid longitudinal acceleration at the solid particle position may substantially increase as the Stokes number goes from 1 to 15, whereas, as seen in Figure 3, the peak of solid particle acceleration RMS first increases from $St = 1$ to 5, and then decreases as the Stokes number is further increased. Clearly, due to the wall, inertial particles are not freely expelled towards regions of low fluid accelerations, as it is the case in HIT.[9,10,33] Instead, with increasing response times, those particles may be subjected to intermittency of high-and-low speed streaks, with strong variations of fluid velocity in the streamwise direction. As the Stokes number becomes bigger, say bigger than $St = 5$ in our DNS, particles respond less and less to varying fluid solicitations. This results in a net decrease in solid particle longitudinal acceleration RMS.

2. Acceleration PDF

In Figure 6, we compare the normalized PDFs of longitudinal and vertical acceleration at $y^+ = 103$ for different Stokes numbers with the normalized PDFs obtained by using the fluid acceleration on the particle position. For reference, the normalized PDF for the unconditional fluid acceleration is plotted as well. As expected, when the Stokes number is increased, the tails of the normalized solid particle PDFs become narrower. For all Stokes numbers, the normalized PDFs of the fluid seen by the solid particles overlap almost perfectly with the normalized PDFs of the unconditional fluid. The same conclusions can be drawn for other distances

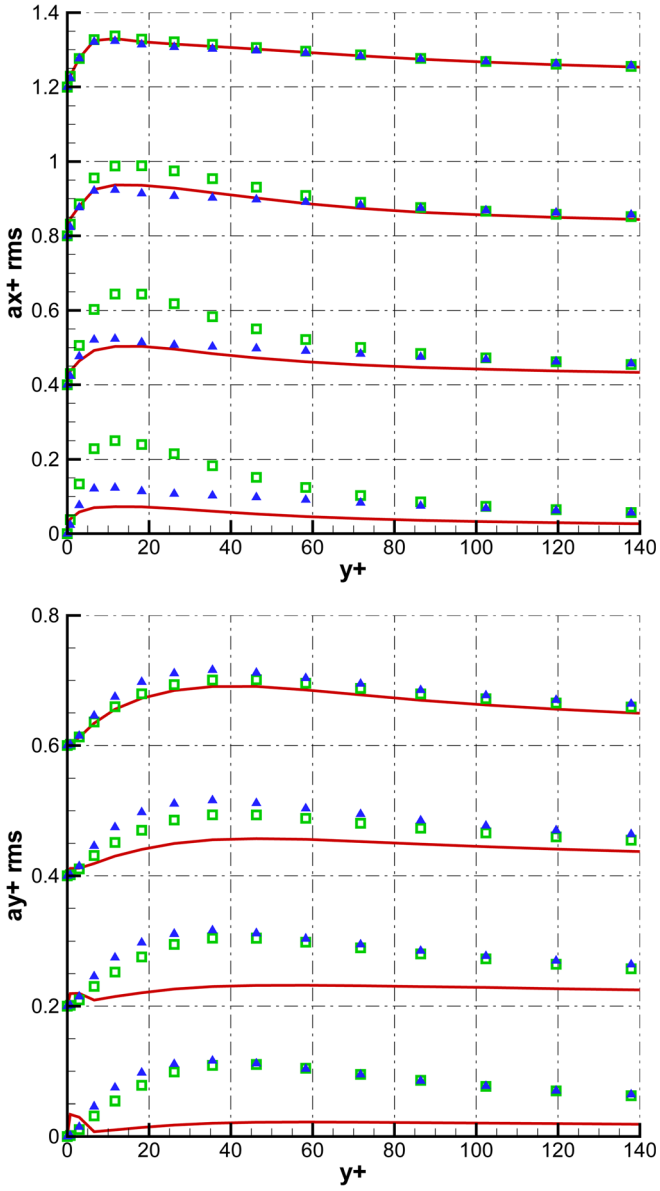

FIG. 5. (Color online) Longitudinal (up) and vertical (bottom) acceleration RMS as a function of y^+. For each plot from top to bottom: $St = 1$, 5, 15, and 25. All plots are shifted up by 0.4 (up) and 0.2 (bottom) units. Solid particles (line), fluid (triangles), fluid at solid particle position (squares).

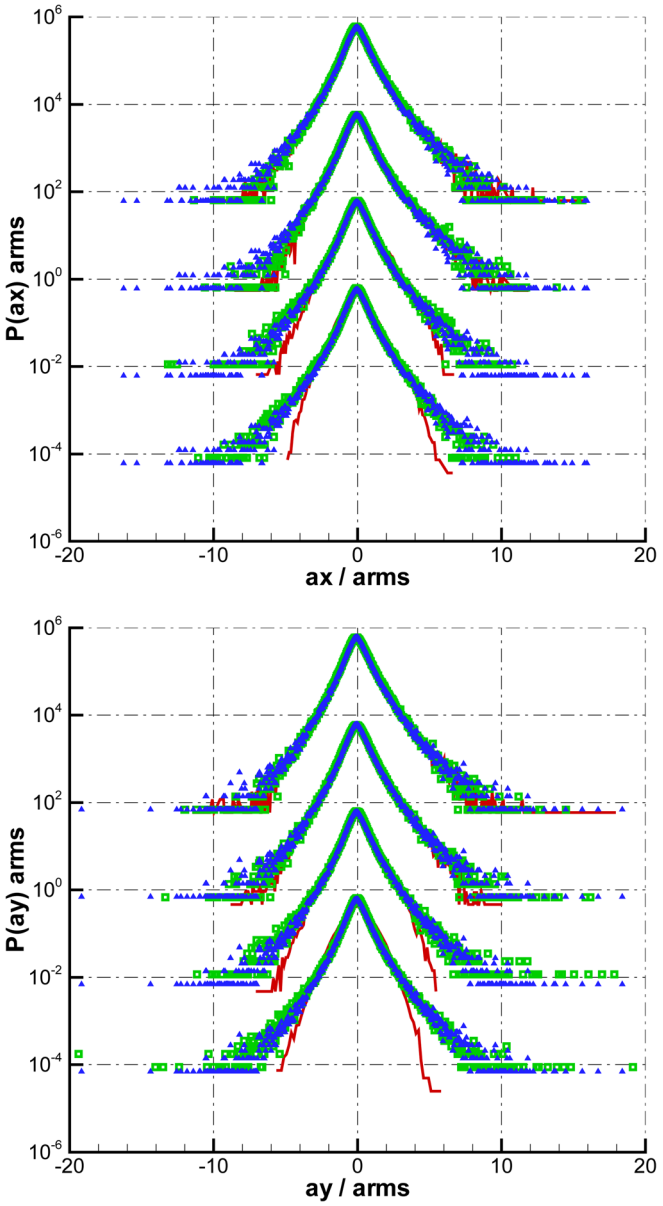

FIG. 6. (Color online) Normalized PDFs of longitudinal (up) and vertical (bottom) acceleration for $y^+ = 103$. For each plot from top to bottom: $St = 1$, 5, 15, and 25. All plots are shifted up by 100 units. Solid particles (line), fluid (triangles), fluid at solid particle position (squares).

to the wall and for the transverse component of the acceleration. As stated above, for clarity of presentation, these plots are not shown here. The overlap suggests scaling symmetry in distributions of conditional and unconditional fluid acceleration. The scaling factor is given by the acceleration RMS, which is different for each Stokes number.

3. Acceleration autocorrelation

The longitudinal and vertical acceleration autocorrelations along the particle trajectory are presented in Figure 7. Due to the inhomogeneous flow condition, the definition of the autocorrelation coefficient must be specified. We choose,

$$\rho_{a_i,a_j}(y_0,t) = \frac{\langle a_i'(t_0)a_j'(t_0+t)\rangle_{y0}}{\left(\langle a_i'(t_0)^2\rangle_{y0}\langle a_j'(t_0+t)^2\rangle_{y0}\right)^{1/2}}, \qquad (6)$$

with a_i' the acceleration fluctuation: $a_i'(t_0+t) = a_i(t_0+t) - \langle a_i(t_0+t)\rangle_{y0}$, and $\langle\bullet\rangle_{y0}$ the mean over the set of particles located at a distance y_0 from the wall at the time t_0 i.e.,: $\langle a_i(t_0+t)\rangle_{y0} = \langle a_i(t_0+t)|y_0\rangle$.

Autocorrelations for the conditional and the unconditional fluid acceleration coincide suggesting the same scaling as the one observed in Figure 6. We may note that for the solid particle autocorrelation, an expected trend is seen: when particle inertia increases, the solid particle acceleration autocorrelation decreases much more slowly, for both components. This is in accordance with previous DNS in HIT.[33]

These results show that in wall-bounded flows, along with effects predicted by Ref. 9 in HIT, there is an additional effect that may increase the particle longitudinal acceleration variance. This effect may be linked to the spanwise intermittency of high-and-low speed streaks aligned with the channel

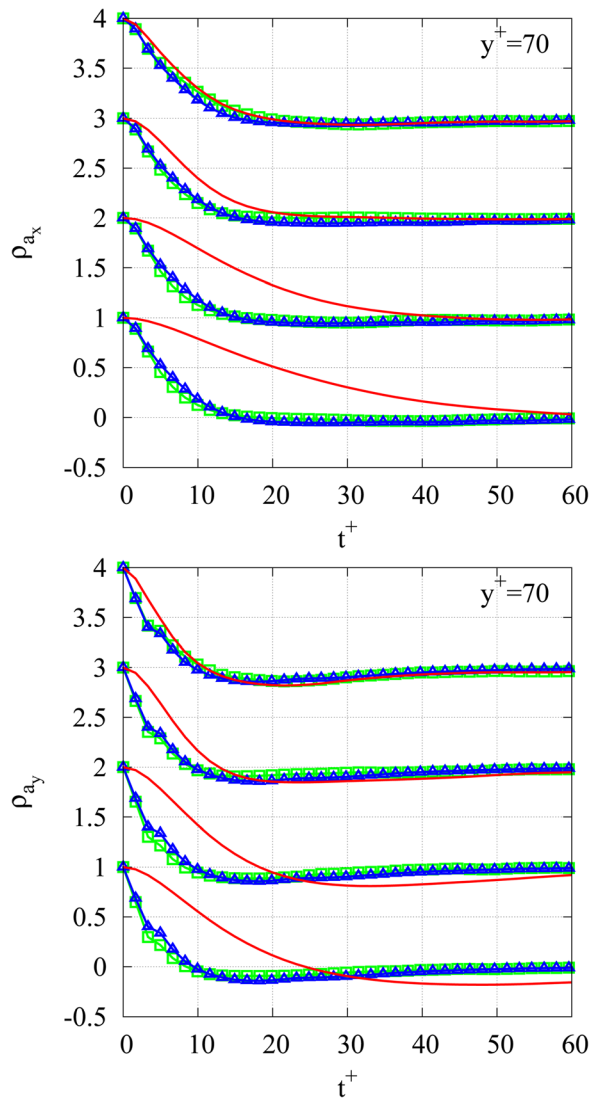

FIG. 7. (Color online) Longitudinal (up) and vertical (bottom) acceleration autocorrelation as a function of time for $y^+ = 70$. For each plot from top to bottom: $St = 1$, 5, 15, and 25. All plots are shifted up by 1 unit. Solid particles (line), fluid (triangles), fluid at solid particle position (squares).

wall. Since inertial particles are swept by these structures, the fluid along the particle path is characterized by enhanced longitudinal acceleration fluctuations. Weakly inertial particles (with a response time τ_p similar to the characteristic fluid timescale) may respond to the fluid variations and therefore experience an increase in the longitudinal acceleration RMS relatively to the fluid. Due to the filtering effect of inertia, strongly inertial particles ignore these wall turbulent structures and, therefore, present a more homogeneous concentration.

V. CONCLUSION

DNS of a turbulent channel flow with Lagrangian particle tracking is used here to study acceleration statistics of inertial particles in the near-wall region and to characterize the fluid acceleration seen by particles. The study is motivated by observations in HIT (Refs. 9, 10, and 34–36) suggesting that the trend of particle acceleration PDF to Gaussianity as well as the decrease in the variance of the acceleration are due to both particle preferential accumulation in quiescent flow regions and particle filtering by inertia. It is shown that the particle acceleration statistics obtained by DNS are in good qualitative agreement with previous studies on this issue.[17,20] As expected, at the channel center, when inertia increases the solid particle PDFs depart from the fluid. The tails of these PDFs become narrower. In addition to this, when particle inertia increases, the solid particle acceleration autocorrelation decreases slower. These results are in accordance with previous studies in HIT.[9,10,34–36]

Complementary to predictions in HIT, it is observed that in the near-wall region, when the Stokes number increases from $St = 1$ to 5, the streamwise acceleration RMS is also increased, while the further increase of the Stokes number leads to a decrease of particle acceleration variance. The peak of the longitudinal acceleration RMS for $St = 1$ and 5 is even higher than the local longitudinal acceleration RMS of the fluid. By analyzing the acceleration statistics of the fluid seen by the solid particles it is found that: (1) contrary to predictions in HIT, while the vertical and transverse acceleration RMS components remain close to the unconditional fluid acceleration, the longitudinal component is remarkably higher. This feature is more pronounced as the Stokes number is increased. (2) The normalized acceleration PDFs overlap almost perfectly with the unconditional fluid normalized PDFs. Particles in their own non-inertial frame of reference see the same statistics of normalized acceleration with a scaling factor depending on inertia. These results may be useful in attempting to infer the statistical information on subgrid scales in turbulent flow simulations with dispersed particles.

The enhanced longitudinal acceleration variance in the fluid around the particle may be due to the spanwise alternation of high-and-low speed streaks. Depending on their inertia, particles may well respond to those fluid solicitations (experiencing an increase of the longitudinal acceleration RMS) or ignore the wall turbulent structures (presenting in that case a more homogeneous concentration). Further studies, inspired by the experimental results of Lelouvetel *et al.*[4] are presently conducted to verify the physical mechanism proposed here.

A few questions arise. Contrary to HIT, the solenoidal component of the acceleration becomes as significant as the potential one in the near-wall region of wall-bounded flows.[37] Yeo *et al.*[31] observed that the streamwise vortex induces a shear zone, resulting in a peak of the solenoidal part of longitudinal acceleration RMS, in the viscous sublayer. For additional analysis of the flow regions where particles tend to cluster, the acceleration of the fluid seen by the solid particles will be decomposed on its potential and solenoidal parts. The influence of each of these two parts will be studied in the future work.

By comparing DNS and experimental data in the case of HIT, Volk *et al.*[35] and Calzavarini *et al.*[33] showed that, when the particle size is larger than the dissipative scale of the flow, the finite size of particles influences their statistical properties. Impact of the particle finite size on the acceleration statistics is also an open question.

In this study, the significance of wall structures on particle acceleration statistics has been shown. Therefore, in the frame of large eddy simulation, prediction of particle dispersion near the wall could be improved by modelling the acceleration of the fluid seen by solid particles at subgrid scales.

ACKNOWLEDGMENTS

M. Buffat is acknowledged for the development of the computational code. The authors express their gratitude to F. Laadhari, who kindly provided his initial fields for the DNS. We thank Z. Warhaft, S. Gerashchenko, V. Lavezzo, and C. Lee for sharing their data with us. This work was granted access to the HPC resources of CINES under the allocation 2009-c200902560 made by GENCI (Grand Equipement National de Calcul Intensif). Numerical simulations were also performed on the P2CHPD parallel cluster; the authors are grateful to C. Pera for the administration of this system.

[1]D. Kaftori, G. Hestroni, and S. Banerjee, "Particle behaviour in the turbulent boundary layer. I. Motion, deposition and entrainment," Phys. Fluids **7**(5), 1095 (1995).
[2]D. Kaftori, G. Hestroni, and S. Banerjee, "Particle behaviour in the turbulent boundary layer. II. Velocity and distribution profiles," Phys. Fluids, **7**(5), 1107 (1995).
[3]J. Kulick, J. Fessler, and J. Eaton, "Particle response and turbulence modification in fully developed channel flow," J. Fluid Mech. **277**, 109 (1994).
[4]J. Lelouvetel, F. Bigillon, D. Doppler, I. Vinkovic, and J.-Y. Champagne, "Experimental investigation of ejections and sweeps involved in particle suspension," Water Resour. Res. **45**, W02416 (2009).
[5]C. Marchioli and A. Soldati, "Mechanisms for particle transfer and segregation in a turbulent boundary layer," J. Fluid Mech. **468**, 283 (2002).
[6]I. Vinkovic, D. Doppler, J. Lelouvetel, and M. Buffat, "Direct numerical simulation of particle interaction with ejections in turbulent channel flows," Int. J. Multiphase Flow **37**, 187 (2011).
[7]K. Kiger and C. Pan, "Suspension and turbulence modification effects of solid particulates on a horizontal turbulent channel flow," J. Turbul. **3**, 1 (2002).
[8]F. Toschi and E. Bodenschatz, "Lagrangian properties of particles in turbulence," Annu. Rev. Fluid Mech. **41**, 375 (2009).
[9]J. Bec, L. Biferale, G. Boffetta, A. Celani, M. Cencini, A. Lanotte, S. Musacchio, and F. Toschi, "Acceleration statistics of heavy particles in turbulence," J. Fluid Mech. **550**, 349 (2006).
[10]S. Ayyalasomayajula, Z. Warhaft, and L. Collins, "Modeling inertial particle acceleration statistics in isotropic turbulence," Phys. Fluids **20**, 095104 (2008).
[11]I. Vinkovic, C. Aguirre, M. Ayrault, and S. Simoëns, "Large-eddy simulation of the dispersion of solid particles in a turbulent boundary layer," Boundary-Layer Meteorol. **121**, 283 (2006).
[12]I. Vinkovic, C. Aguirre, S. Simoëns, and M. Gorokhovski, "Large eddy simulation of droplet dispersion for inhomogeneous turbulent wall flow," Int. J. Multiphase Flow **32**, 344 (2006).
[13]V. Sabel'nikov, M. Gorokhovski, and N. Baricault, "The extended IEM mixing model in framework of the composition pdf approach: Applications to diesel spray combustion," Combust. Theory Modell. **10**, 155 (2006).
[14]M. Bourgoin, N. Ouellette, H. Xu, J. Berg, and E. Bodenschatz, "The role of pair dispersion in turbulent flow," Science **311**, 835 (2006).
[15]G. Voth, A. LaPorta, A. Carwford, J. Alexander, and E. Bodenschatz, "Measurements of particle accelerations in fully developed turbulence," J. Fluid Mech. **469**, 121 (2002).
[16]N. Mordant, P. Metz, O. Michel, and J.-F. Pinton, "Measurement of Lagrangian velocity in fully developed turbulence," Phys. Rev. Lett. **87**, 214501 (2001).
[17]V. Lavezzo, A. Soldati, S. Gerashchenko, Z. Warhaft, and L. Collins, "On the role of gravity and shear on inertial particle accelerations in near-wall turbulence," J. Fluid Mech. **658**, 229 (2010).
[18]V. Kuznetsov and V. Sabel'nikov, *Turbulence and Combustion*, revised and augmented for the English edition (Hemisphere Publishing Corporation, New York, 1990).
[19]J. K. Eaton and J. R. Fessler, "Preferential concentration of particles by turbulence," Int. J. Multiphase Flow **20**, 169 (1994), Turbulence.
[20]S. Gerashchenko, N. Sharp, S. Neuscamman, and Z. Warhaft, "Lagrangian measurements of inertial particle accelerations in a turbulent boundary layer," J. Fluid Mech. **617**, 255 (2008).
[21]R. Clift, J. Grace, and M. Weber, *Bubble, Drops, and Particles* (Academic Press, Singapore, 1978).
[22]H. Pascal, "*Étude d'une turbulence compressée ou cisaillée entre deux plans parallèles: comparaison entre approche statistique et simulation des équations de Navier-Stokes instantanées*," Ph.D. dissertation (École Centrale de Lyon, 1996).
[23]M. Buffat, L. L. Penven, and A. Cadiou, "An efficient spectral method based on an orthogonal decomposition of the velocity for transition analysis in wall bounded flow," Comput. Fluids **42**, 62 (2011).
[24]F. Laadhari, "On the evolution of maximum turbulent kinetic energy production in a channel flow," Phys. Fluids **14**, L65 (2002).
[25]F. Laadhari, "Reynolds number effect on the dissipation function in wall-bounded flows," Phys. Fluids **19**, 038101 (2007).
[26]R. Moser, J. Kim, and N. Mansour, "Direct numerical simulation of turbulent channel flow up to $Re_\tau = 590$," Phys. Fluids **11**, 943 (1999).
[27]S. Hoyas and J. Jiménez, "Reynolds number effects on the Reynolds-stress budgets in turbulent channels," Phys. Fluids **20**, 101511 (2008).
[28]R. Zamansky, I. Vinkovic, and M. Gorokhovski, "LES approach coupled with stochastic forcing of subgrid acceleration in a high-Reynolds-number channel flow," J. Turbul. **11**, 30 (2010).
[29]J.-I. Choi, K. Yeo, and C. Lee, "Lagrangian statistics in turbulent channel flow," Phys. Fluids **16**, 779 (2004).
[30]N. Mordant, A. M. Crawford, and E. Bodenschatz, "Experimental Lagrangian acceleration probability density function measurement," Physica D **193**, 245 (2004).
[31]K. Yeo, B.-G. Kim, and C. Lee, "On the near-wall characteristics of acceleration in turbulence," J. Fluid Mech. **659**, 405 (2010).
[32]C. Marchioli, A. Soldati, J. Kuerten, B. Arcen, A. Tanière, G. Goldensoph, K. Squires, M. Cargnelutti, and L. Portela, "Statistics of particle dispersion in direct numerical simulations of wall-bounded turbulence: Results of an international collaborative benchmark test," Int. J. Multiphase Flow **34**, 879 (2008).
[33]E. Calzavarini, R. Volk, M. Bourgoin, E. Lévêque, J.-F. Pinton, and F. Toschi, "Acceleration statistics of finite-sized particles in turbulent flow: The role of Faxén forces," J. Fluid Mech. **630**, 179 (2009).
[34]S. Ayyalasomayajula, A. Gylfason, L. Collins, E. Bodenschatz, and Z. Warhaft, "Lagrangian measurements of inertial particle accelerations in grid generated wind tunnel turbulence," Phys. Rev. Lett. **97**, 144507 (2006).
[35]R. Volk, E. Calzavarini, G. Verhille, D. Lohse, N. Mordant, J.-F. Pinton, and F. Toschi, "Acceleration of heavy and light particles in turbulence: Comparison between experiments and direct numerical simulations," Physica D **237**, 2084 (2008).
[36]N. Qureshi, U. Arrieta, C. Baudet, A. Cartellier, Y. Gagne, and M. Bourgoin, "Acceleration statistics of inertial particles in turbulent flow," Eur. Phys. J. B **66**, 531 (2008).
[37]C. Lee, K. Yeo, and J.-I. Choi, "Intermittent nature of acceleration in near-wall turbulence," Phys. Rev. Lett. **92**, 144502 (2004).